Anatase TiO2 nanoparticles for lithium-ion batteries

S. S El-Deen, A. M Hashem, A E Abdel Ghany, S. Indris, H. Ehrenberg, A. Mauger, C. Julien

▶ **To cite this version:**

S. S El-Deen, A. M Hashem, A E Abdel Ghany, S. Indris, H. Ehrenberg, et al.. Anatase TiO2 nanoparticles for lithium-ion batteries. Ionics, In press, 10.1007/s11581-017-2425-y . hal-01693653

HAL Id: hal-01693653

https://hal.sorbonne-universite.fr/hal-01693653

Submitted on 26 Jan 2018

HAL is a multi-disciplinary open access archive for the deposit and dissemination of scientific research documents, whether they are published or not. The documents may come from teaching and research institutions in France or abroad, or from public or private research centers.

L'archive ouverte pluridisciplinaire **HAL**, est destinée au dépôt et à la diffusion de documents scientifiques de niveau recherche, publiés ou non, émanant des établissements d'enseignement et de recherche français ou étrangers, des laboratoires publics ou privés.

Anatase TiO_2 nanoparticles for lithium-ion batteries

S.S. El-Deen[1], A.M. Hashem[2,3], A.E. Abdel Ghany[2,4], S. Indris[3], H. Ehrenberg[3], A. Mauger[4], C.M. Julien[4]

[1]Department of Nuclear Chemistry, Hot Laboratories Center, Atomic Energy Authority, Inshas P.O. Box 13759, Egypt

[2]National Research Centre, Inorganic Chemistry Department, 33 El Bohouth st. (former El Tahrir st.), Dokki Giza, P.O. 12622, Egypt

[3]Karlsruhe Institute of Technology (KIT), Institute for Applied Materials -Energy Storage Systems (IAM- ESS), Hermann-von-Helmholtz-Platz 1, D-76344 Eggenstein-Leopoldshafen, Germany

[4]Sorbonne Universités, Institut de Minéralogie, de Physique des Matériaux et de Cosmologie (IMPMC), UMR 7590, 4 place Jussieu, 75005 Paris, France

Corresponding author: christian.julien@upmc.fr (C.M. Julien)

Abstract

Anatase TiO_2 nanoparticles were prepared by a simple sol-gel method at moderate temperature. X-ray powder diffraction (XRD) and Raman spectroscopy revealed the exclusive presence of anatase TiO_2 without impurities such as rutile or brookite TiO_2. Thermogravimetric analysis confirmed the formation of TiO_2 at about 400 °C. Particles size of about 20 nm observed by transmission electron microscopy matches well with the dimension of crystallites calculated from XRD. The electrochemical tests of the sol-gel prepared anatase TiO_2 show promising results as electrode for lithium-ion batteries with a stable specific capacity of 174 mAh g^{-1} after 30 cycles at C/10 rate. The results show that improvement of the electrochemical properties of TiO_2 to reach the performance required for use as an electrode for lithium-ion batteries require not only nano-sized porous particles, but also a morphology that prevents the self-aggregation of the particles during cycling.

Keywords: TiO_2 anatase; nanoparticles; Raman spectroscopy; electrode material; lithium-ion batteries.

Introduction

Special attention was directed to rechargeable lithium batteries as important primary (non-rechargeable) and secondary (rechargeable) electrochemical cells to power most of portable electronic devices such as cell phones, cameras, laptops, etc. Nowadays, lithium-ion batteries (LiBs) are regarded as electrochemical power sources in electric (EVs) and hybrid-electric (HEVs) vehicles due to their high energy and power densities, long cyclability and the absence of a memory effect [1,2].

Current cathode materials of commercial lithium batteries are $LiCoO_2$, $LiFePO_4$ or $LiMn_2O_4$, while the graphite or carbonaceous materials are chosen as anode materials [3]. However, graphitic anode material cannot meet all the commercial requirements for important applications because limitation coming from some drawbacks such as initial capacity loss and structural modification during electrochemical cycling [4-6]. Consequently, scalable syntheses of low cost and new electrode materials delivering stable and high specific capacity are desirable. Actually, several transition-metal oxides are under investigation for this purpose such as NiO [7, 8], Co_3O_4 [8], CuO [8], Fe_2O_3 [9-12] and TiO_2 [13-16].

Titanium dioxide (TiO_2) has various applications in solar cells [17-21], photo-electrochemical sensor [22], photo catalysis [23-26] and energy storage [27]. Nanostructured TiO_2 as electrode materials for Li-ion batteries is recognized for its unique electrochemical properties. This oxide has outstanding properties such as high theoretical capacity (335 mAh g^{-1}), low cost, high safety, low toxicity, good cycling life, convenient discharge potential (<2.0 V), slight volume change (3–4%) during lithium intercalation and fast ionic transport especially in nano-structured form [28-30]. These advantages have discussed recently in [3]. Among the different polymorphs forms of TiO_2, e.g. rutile ($P4_2/mnm$ S.G.), anatase ($I4_1/amd$ S.G.), brookite (*Pbca* S.G.), bronze TiO_2-B (*C2/m*), ramdellite (*Pbnm* S.G.), etc. the anatase lattice can accommodate 0.5Li per formula unit with good insertion kinetics, while rutile and brookite frameworks can uptake few percents of Li^+ ions during the insertion/deinsertion reaction [31,32].

It is well known that the decrease of the particle size from micron- to nano-scale can enhance the specific capacities and the rate capability due to the shorter pathway L for ions and electrons and an increase of the surface area A of the interface between electrode and electrolyte. Higher A diminishes the overpotential and increases the reaction at the interface, while smaller L favors the characteristic times τ for kinetics in the proportion $\tau=L^2/\pi D^+$ with D^+ the diffusion coefficient of ions [3,28]. The growth of nanosized TiO_2 powders can be

obtained using different synthesis routes such as co-precipitation [33-36], sol-gel [13], emulsion [16] and hydrothermal methods [31].

In this work, we study the nanosized TiO_2 material synthesized via sol-gel technique. The synthesized oxide was investigated by several tools such as X-ray diffraction (XRD), thermogravimetry analysis (TGA), Raman spectroscopy (RS) and transmission electron microscopy (TEM). Further electrochemical properties of anatase TiO_2 were carried out by cyclic voltammetry, galvanostatic charge-discharge and cycling tests as electrode material in lithium-ion battery.

Experimental

TiO_2 nanoparticles were prepared by the sol-gel method according to the method desvribed by Deedar et al. [36], using titanium iso-propoxide (TIP) ($C_{12}H_{28}O_4Ti$) as raw materials. The mixture of TIP (108 ml) and n-propanol (252.5 ml) was stirred for 5 min using a magnetic stirrer at 500 rpm. In the next step, HCl (2 ml) was added to n-propanol (25.5 ml) at the rate of 1 ml/min. (molar ratio of HCl/TIP was 0.2). After stirring for 30 min, 160.3 ml of the mixture was diluted in 25.3 ml of water at a rate of 1 ml/min. The molar ratio of H_2O/TIP was 4. Then, the mixture was stirred for 24 h at room temperature to form a gel, which was dried overnight. Subsequently, the gel was calcined at 400 °C for 1 h in a muffle-type furnace to obtain the nanosized TiO_2 anatase particles.

XRD patterns were collected using a Philips X'Pert apparatus equipped with a CuK_α X-ray source (λ = 1.54056 Å) in the 2θ range 10–80°. Raman scattering (RS) spectra were recorded using a LabRam Evolution HR (HORIBA) spectrometer equipped with a Nd:YAG laser (523 nm, 1 mW). The spectra were recorded using a backscattering geometry, and the laser power was kept below 25 mW to prevent the degradation of materials by the laser during data acquisition (spectral resolution of 2 cm^{-1}). TGA measurements were carried out using a thermal gravimetric analyzer (Perkin Elmer, TGA 7 series) in the temperature range of 30–1000 °C in air at a heating rate of 10 °C min^{-1}. A JEOL, transmission electron microscope (TEM, JEM-1230, Japan) was used to investigate the structure and morphology of nanoparticles.

TiO_2 electrodes were prepared from a mixture 80% (w/w) of the active material, 10% (w/w) super C65 carbon (TIMCAL) and 10% (w/w) polyvinylidene fluoride (Solef PVdF 6020 binder, Solvay), in N-methyl-2-pyrrolidone (NMP, Sigma-Aldrich) to get a slurry. Typical electrode with a thickness of 90 nm obtained by coating the slurry on Al foil at a

loading of ~7 mg cm^{-2} was dried over night at 80 °C; then discs were punched out with a diameter of 1.2 cm. Further drying for the electrode disks at 100 °C under vacuum was done and finally it was compacted with a pressure of 8 tons. The cell was assembled using two-electrode Swagelok®- type test cells in an argon-filled glove box with lithium foil (Alfa Aesar) as anode, LP30 1mol L^{-1} $LiPF_6$ in (1:1) ethylene carbonate (EC) and dimethyl carbonate (DMC) as electrolyte, and glass microfiber filters (Whatmann®-GF/D 70 mm Ø) as separator. A VMP3 multi-channel potentiostat (Bio-Logic, France) was used for the electrochemical tests of the electrodes at 25 °C in the voltage range of 1-3 V with galvanostatic cycling (C/10 rate) and cyclic voltammetry (CV) at 0.05 mV s^{-1} sweep rate.

Results

Structure and Morphology

The XRD pattern of TiO_2 calcined at 400 °C shown in Fig. 1 reveals the presence of characteristic peaks at 2θ values of 25.42, 37.89, 48.12, 54.04, 55.16 and 62.79°, corresponding to (101), (004), (200), (105), (211) and (204) crystal planes of the tetragonal phase of TiO_2, space group $I4_1/amd$, respectively [31]. This result clarifies that TiO_2 has exclusively grown in the anatase phase and it matches well with pattern of the database (JCPDS 21-1272). The rather broad peaks indicate the nano-sized character of the crystallites. No peak corresponding to rutile phase was observed. Rietveld refinement has been performed as follows. We start with the constraints that, at ideal stoichiometry, Ti ions occupy the 4*a* Wyckoff position while the oxygen anions occupy the 8*e* sites. The best fit (Fig. 1) was obtained with R_{wp}=11.43%, χ^2=1.191, $R(F^2)$=0.125 and the lattice parameters are determined as $a=b$=3.7864 Å and c=9.5142 Å. The average crystallite size of ~22 nm was calculated via the Scherrer's equation using the full-width at half-maximum (FWHM) of seven Bragg peaks.

The thermogravimetric analysis (TGA) of precursor and as-prepared TiO_2 is displayed in Fig. 2. For the precursor about 22.3% weight loss was observed till 450 °C and the profile was flat above this temperature. It means that the residual water and organic residues were eliminated below 400 °C. The weight loss between room temperature and 200 °C is mainly due to removal of alcohol and adsorbed water. The weight loss between 200 and 400 °C is attributed to the elimination of organic materials and formation of pure TiO_2 nanoparticles [38] as confirmed by our TGA data (Fig. 2). The sample prepared at 400 °C for 1 hour shows only a slight weight loss (2.3%) below 450 °C due to surface water followed by almost no

weight loss, which indicates a high thermal stability of the TiO_2 anatase nanoparticles up to 1000 °C.

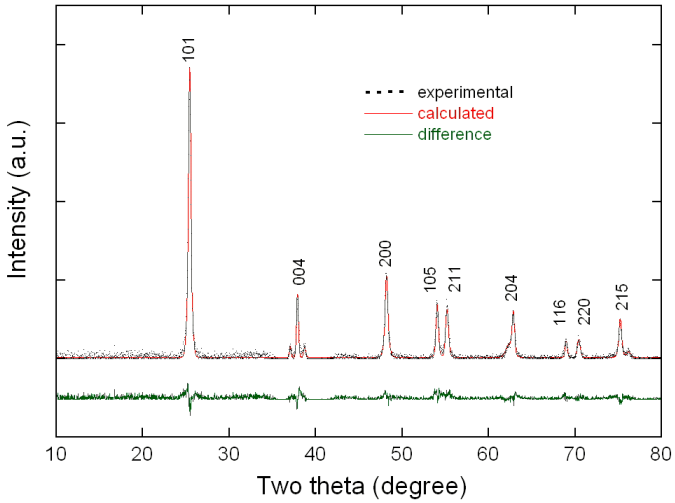

Figure 1. Rietveld refinement of XRD pattern of TiO_2 nanoparticles heat treated at 400 °C. The Bragg lines are indexed in the tetragonal structure (space group $I4_1/amd$).

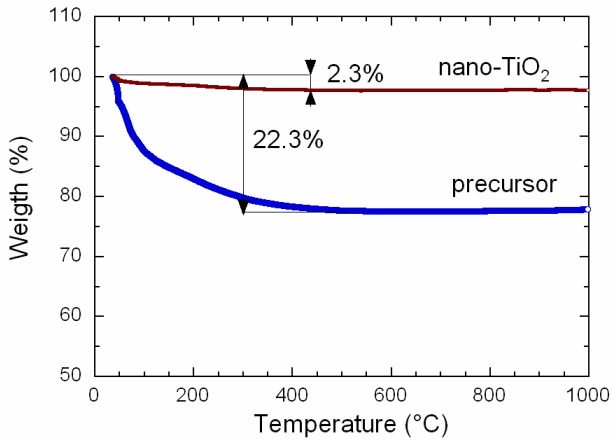

Figure 2. Thermogravimetric analysis of the precursor and the sol-gel as-prepared anatase TiO_2 nanoparticles.

To confirm the high purity of the TiO_2 anatase nanoparticles, the Raman spectrum (RS), which is a sensitive tool, was carried out to give a better insight into the structure of synthesized TiO_2 nanoparticles (Fig. 3). The space group of the tetragonal anatase is $I4_1/amd$ and the local symmetry is D_{2d} [39]; The group factor analysis provides six basic Raman-active modes with the representation as $A_{1g} + 2B_{1g} + 3E_g$ in contrast to four active modes

A_{1g}+B_{1g}+B_{2g}+E_g for the rutile phase [40,41]. The RS spectrum shown in Fig. 3 evidences the typical features of the TiO_2 anatase with the bands at 144 (E_g), 197 (E_g), 399 (B_{1g}), 513 (A_{1g}), 519 (B_{1g}) and 639 cm^{-1} (E_g). Thus, a good agreement is observed between RS and XRD data, which confirms the high purity TiO_2 anatase phase prepared by the sol-gel synthesis at moderate temperature.

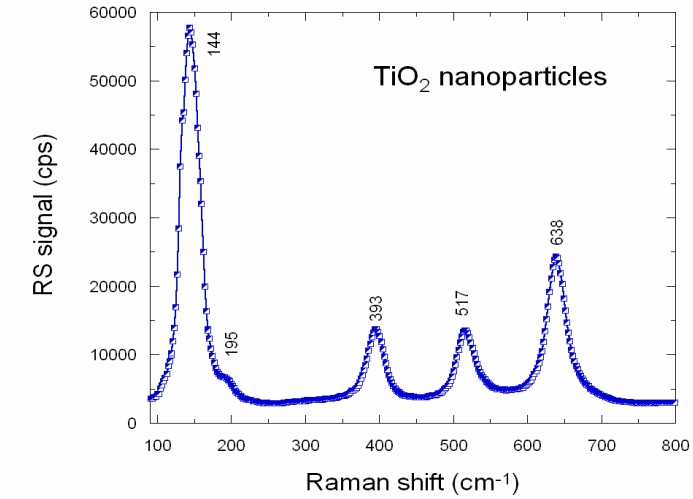

Figure 3. Raman spectrum of the as prepared anatase TiO_2 recorded with the 514.5 nm excitation wavelength.

Figure 4 displays the TEM image (a), the electron diffraction diagrams (b) and the HRTEM image (scale=20 nm) (c) of TiO_2 powder prepared at 400 °C. The nanoparticles of regular shape are well dispersed with slight agglomeration. Each grain has an average particle size of about 20 nm, which is consistent with the dimension of crystallites calculated from XRD. The electron diffraction patterns show the nanometer sized character of TiO_2 particles.

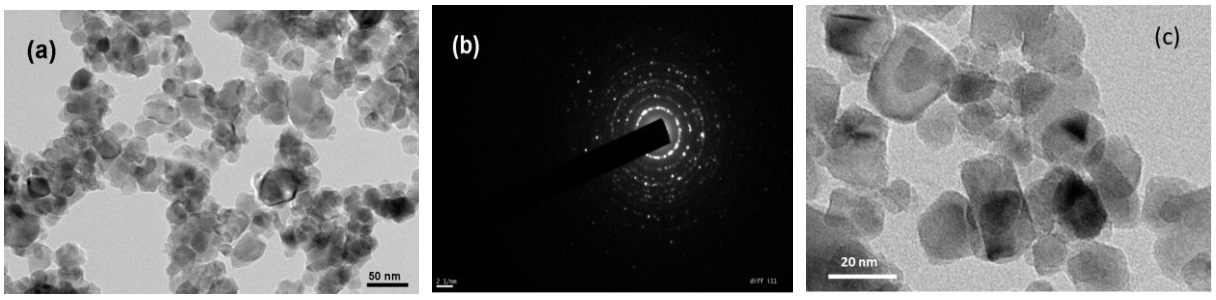

Figure 4. (a) TEM image and (b) electron diffraction diagram of anatase TiO_2 nanoparticles heat treated at 400 °C. (c) HRTEM image (scale=20 nm).

Electrochemical properties

The electrochemical performance of TiO_2 was evaluated in half-cell configuration (Li//TiO_2) in the potential range 1-3 V vs. Li^+/Li^0 at room temperature. The cyclic voltammetry test for the first five cycles is displayed in Fig. 5. The cell was first discharged to enable insertion of lithium ions into the TiO_2 crystal lattice, resulting in a reduction of titanium ions. Sharp peaks at ~1.70 and ~2.02 V were observed during cathodic and anodic reaction, respectively. The separation of anodic and cathodic peaks is ubiquitous in crystalline anatase electrodes. These peaks are assigned to the reduction of Ti^{4+} to Ti^{3+} during the discharge and subsequent oxidation to +4 during charge, which indicates the excellent reversibility of the anatase TiO_2 as an insertion host. Electrochemical lithium insertion/extraction can be expressed by the following insertion-deinsertion reaction: $TiO_2 + xLi^+ + xe^- \leftrightarrow Li_xTiO_2$ [42]. However, in the subsequent cycles, small deviations in the peak positions are noted, possibly due to some stress in the TiO_2 crystal lattice.

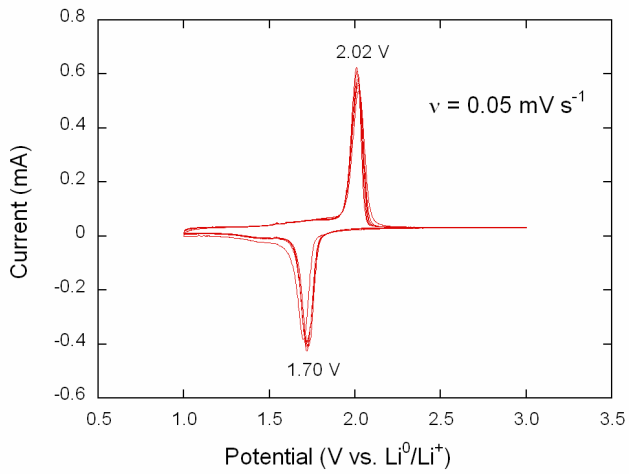

Figure 5. Cyclic voltammogram of TiO_2 in half-cell cycled in the range 1-3 V vs. Li^+/Li^0 at sweep rate of 0.05 mV s^{-1}.

Figure 6 shows the galvanostatic charge–discharge curves of TiO_2 in the potential range 1.0–3.0 V at a 0.1C rate (C rate was calculated on the basis of 1C=335 mAh g^{-1}). An initial discharge capacity of 221 mAh g^{-1} corresponds to insertion of 0.66 mol of Li per formula unit. In the first charge, the cell delivered a reversible capacity of 189 mAh g^{-1} (0.56 mol of Li from the theoretical capacity). Although anatase TiO_2 exhibits a theoretical specific capacity of 335 mAh g^{-1}, the practical capacity attainable is twice smaller, because of the strong Li-Li repulsion in the Li_xTiO_2 framework at greater degree of insertion, i.e. x>0.5 [43]. The irreversible capacity in the first cycle is estimated to be ~32 mAh g^{-1}, which corresponds to~

0.1 mol of lithium. After 30 cycles, the charge and discharge capacity slightly decreased to 182 and 174 mAh g^{-1}, respectively, providing a decreasing irreversible capacity of 8 mAh g^{-1}. The discharge plateau related to the beginning of lithium insertion is observed at ~1.76 V and the charge plateau starts at ~1.9 V for the Li deinsertion. These potentials are similar to those reported in the literature (~1.75 and ~1.88 V, respectively). This behavior matches well with the redox peak mentioned above in the cyclic voltammogram. The electrochemical performance of our sample is comparable with that of the literature. For instance, Rai et al. [28] reported a discharge and charge capacity of ~214 and ~154 mAh g^{-1}, respectively, for TiO_2 nanoparticles (<10 nm) cycled at 0.06C. However, it was reported that during Li insertion, the symmetry of the anatase unit cell decreases and its original tetragonal ($I4_1/amd$) structure transforms into the orthorhombic ($Pmn2_1$) space group [44]. This phase transition occurs in the regime of deep discharge along with a spontaneous phase separation of a lithium-poor ($Li_{0.01}TiO_2$) and a lithium-rich ($Li_{0.5}TiO_2$) phase [45]. Note that (a) the decrease of the irreversible capacity (32 against 8 mAh g^{-1}) means no phase transition but a usual electrochemical behavior, (b) the voltage profile of the active electrode material annealed at 400 °C displays only a small polarization V_{ch}-V_{dis} = 120 mV due to the good crystallinity of particles and (c) the small particle size (L = 20 nm) allows quick Li-ion insertion-deinsertion due to the short distance for Li^+ transport. The rate capability and cycling performance of 20-nm sized TiO_2 particles are presented in Fig. 7. The rate capability has been tested at the 2nd cycle in the C-rate range from C/20 to 50C as displayed by the modified Peukert plot (Fig. 7a). As commonly observed for electrode materials, the decay of the discharge capacity follows a semi-logarithmic law as the current passed through the cell increases. After tests at high C-rate of 10C (corresponding to a full discharge in 6 min), the capacity ~125 mAh g^{-1} is delivered after the 2nd cycle and a capacity of 45 mAh g^{-1} at 30C rate, which gives evidence of the electrochemical reversibility and structural stability of the samples. Figure 7b presents the discharge capacity as a function of the cycle number for cycling between 1 and 3 V at a C/10 rate. The cell showed a very stable cycling after capacity fading in the initial few cycles. The capacity retention of about 82.5% was obtained after 30 cycles. Note that the capacity fading in the initial cycle is due to cell formation (growth of the SEI).

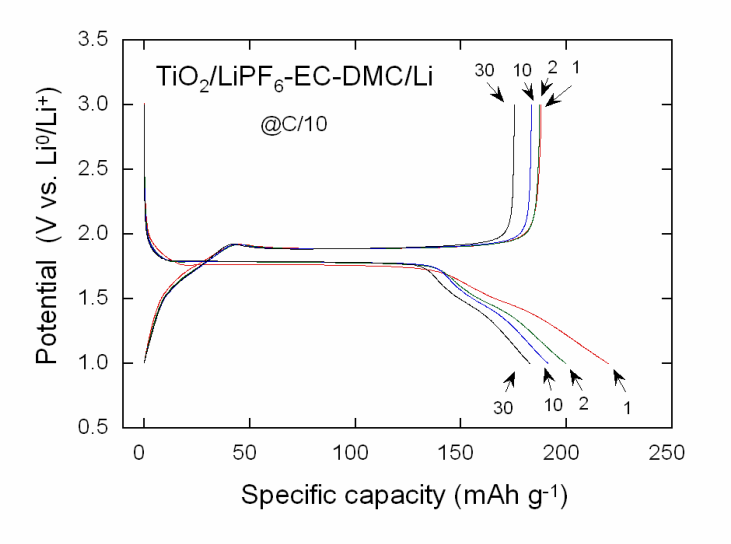

Figure 6. Charge and discharge curves of TiO_2 operated at C/10 rate in the potential range 1-3 V vs. Li^+/Li^0 at room temperature. Cycle numbers are given in the graph.

For comparison, the capacity retention of the nanotubes is 81%, and that of nano-rods is only 40% after 30 cycles [46]. Therefore, the nanoparticles in the present work have reached the same cyclability as the nanotubes, with the advantage that the nanoparticles have been synthesized by a scalable and simple sol-gel synthesis process. We also note that anatase is a better photocatalyst than rutile TiO_2 [47], so that the sol-gel synthesis of anatase TiO_2 has also important applications in this context, as the sol-gel process is also efficient to synthesize thin films [48]. The drawback of the catalytic surface of TiO_2 is that its catalyst sites have side reactions with the organic electrolytes. The fact that our nanoparticles have irreversible capacity loss similar to other nano-structures surfaces such as nanotubes or nanorods using similar electrolytes suggest that it is a general property of this transition metal oxide linked to this catalytic property of the high energy sites at the surface. In particular, Ti-OH units are known to be highly catalytic toward counter-ion (PF_6^-). This drawback may be overcome by coating the TiO_2 anode material with a protective layer. For instance, Tan et al. [49] have recently reported that coating TiO_2 with a uniform and continuous nitrogen-doped carbon layer with thickness of 4±0.5 nm leads to higher discharge retention and better cycling performance.

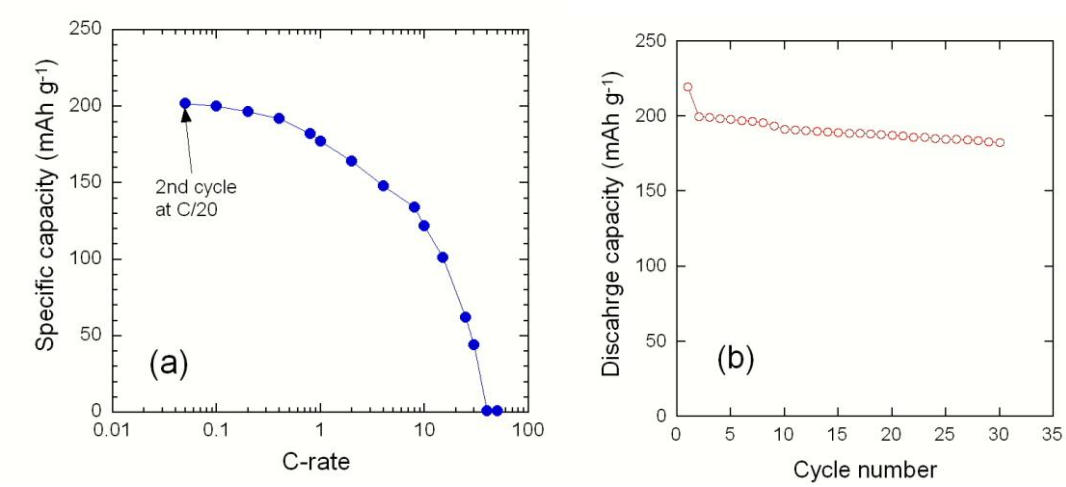

Figure 7. (a) Modified Peukert plot of 20-nm sized TiO_2 particles carried out at the 2nd cycle. (b) Cycling performance of anatase TiO_2 nanoparticles operated at C/10 in the potential range 1-3 V vs. Li metal at room temperature.

The diffusion coefficient D_{Li} of Li^+ ions in anatase TiO_2 nanoparticles has been investigated using cyclic voltammetry at different scan rates (Fig. 8a). The relation between the current I_p and the scan rate ν is expressed by the Randles equation [50]:

$$I_p = 0.4958nFAC^*\left(\frac{D_{Li}\alpha nF}{RT}\right)^{1/2}\nu^{1/2} = \psi_{ox,red}\nu^{1/2}, \qquad (1)$$

where F, R and T are the usual constants, A the surface area of the electrode, C^* the concentration of Li^+ ions (C^*=23.6 mol dm^{-3} assuming a composition $Li_{0.5}TiO_2$), n the number of electrons and α the transfer constant (α=0.5). D_{Li} derived from the plots in Fig. 8b are 8.5×10^{-13} and 5.8×10^{-13} cm^2 s^{-1} for oxidation (Li extraction) and reduction (Li insertion) respectively. These values provide a characteristic time $t=L^2/\pi D_{Li}$ for intercalation of the particles equal to 1 h. Several authors reported the diffusion coefficient of Li^+ ions in anatase TiO_2 nanoparticles as insertion host materials [51-59]. There is general agreement for overall diffusion process dominated by the bulk diffusion, which is considered as rate limiting. The diffusion coefficients evaluated using different techniques: chronoamperometry [51,54,55], galvanostatic titration [52], cyclic voltammetry [53,57,58], NMR [56] and EIS [59] appeared to be in the range 10^{-16}-10^{-12} cm^2 s^{-1}. Our results are in good agreement with those of Kavan et al. [55], who reported a higher D_{Li} for the de-insertion process. This difference in the rate of the insertion/de-insertion process has been attributed to the lattice relaxation during the accommodation of Li^+ ions in the anatase framework. Cantao et al. [52] reported the

logarithmic variation of D_{Li} with the film thickness; the highest diffusion coefficient was obtained for the thicker film. Table 2 summarized the D_{Li} values of the literature.

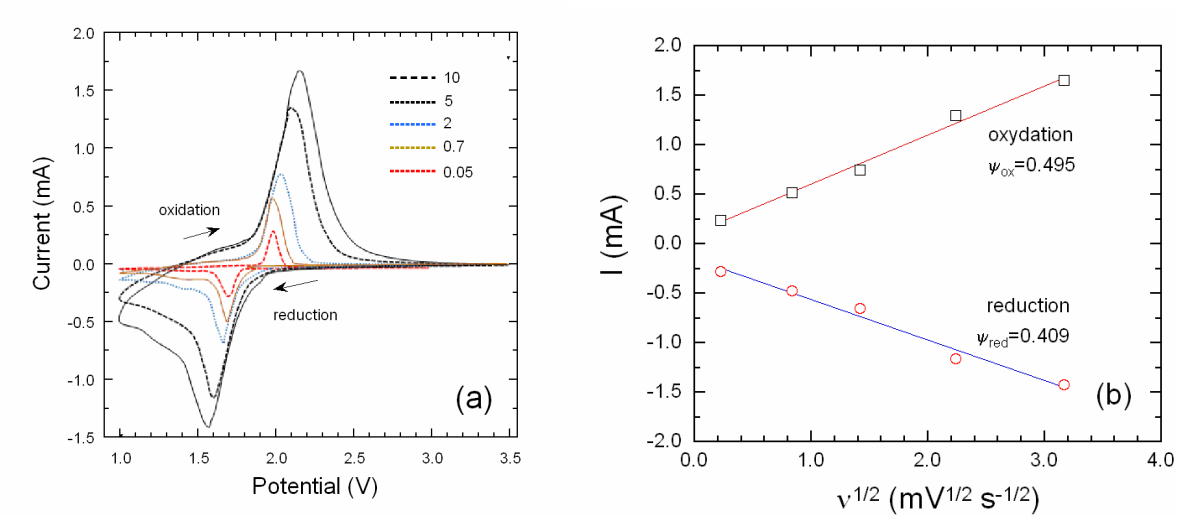

Figure 8. (a) Cyclic voltammogram of TiO_2 as a function of the scan rate from 0.05 to 10 mV s^{-1}. (b) Plot of the current vs. square root of the scan rate for the oxidation and reduction peaks.

Table 1. Diffusion coefficient of Li^+ ions in TiO_2 host materials.

Material	Particle size (nm)	Diffusion coefficient (cm^2 s^{-1})	Reference
Anatase thin films	1.55 µm thick	3.8×10^{-13}	[51]
TiO_2 thin films	25	5.0×10^{-13}	[52]
Anatase nanoporous films	4.2 µm thick	4.0×10^{-17}	[53]
CVD films	2.2 µm thick	2.0×10^{-15}	[54]
Anatase single crystals	-	2.0×10^{-13}	[55]
Anatase (NMR measurements)	60-80	4.7×10^{-12}	[56]
Nano TiO_2(B)	10-20	3.9×10^{-16}	[57]
TiO_2 nanotubes	150 nm dia.	6.1×10^{-16}	[58]
C-coated TiO_2	60	4.6×10^{-13}	[59]
Anatase nanoparticles	20	8.5×10^{-13}	This work

Discussion

The high performance of the anatase TiO_2 particles is linked to their small diameter of 20 nm. However, even if we have decreased the size of the particles to this nanometer range and

obtained particles that are single crystals without any impurity, we find that the problem of the cycling life, which is vital for Li-storage performance and a well-known limiting factor of TiO_2, has not been solved. The first idea to improve the electrochemical properties is to use porous particles to increase the effective surface area in contact with the electrolyte, and coat the particles with carbon. The beneficial effect of carbon coating of TiO_2 has been observed in many works (see [60] for a review). In particular, Fu et al. [61] reported improved electrochemical properties obtained with N-doped carbon coating of TiO_2 spherical particles, using ethylenediamine ($C_2H_6N_2$, EDA) as the N-doped carbon precursor. The beneficial effect of carbon coating nanoparticles of active electrode elements is a general property, that is not only observed in all the Li-ion batteries [3], but also been observed in Na-ion batteries [62-64]. Generally, this improvement comes from the fact that the intrinsic electrical conductivity of the particles is small, so that the coating by conductive carbon improves both the capacity and rate capability. In the particular case of TiO_2, however, another reason for the improvement of the cycling life with N-doped carbon coating [61] may be invoked: a synergetic effect of the increase of the conductivity and an increase of the surface stability by coating with N-doped carbon owing to the strong interaction of TiO_2 with ethylenediamine [65], plus nitridation of Ti atoms to form O-Ti-N bonds. The nitridation should be largely the dominant effect with respect to the EDA-TiO_2 interaction, because outstanding results have been obtained on other N-doped carbon coated TiO_2 without the EDA precursor (one-step synthesis by hydrolyzing tetrabutyl-titanate (TBT) mixed with urea and heated in a sealed autoclave at 550 °C for 5 h) [66].

The next question is to know if it is possible to improve the electrochemical properties by decreasing even more the particle size. For instance, Tan et al. [49] have recently reported that coating TiO_2 with a uniform and continuous nitrogen-doped carbon layer with thickness of 4±0.5 nm leads to higher discharge retention and better cycling performance. To answer this question, we can compare our results with prior works that have been published for particles 4 nm thick, obtained either by fragmentation of nanorods [67], or by a two-step room temperature synthesis process [68,69]. In one case [67], the electrochemical properties are better, as these particles delivered a capacity of 200 mAh g^{-1} for 500 cycles at 1C rate. To the contrary, in the other case [68], the opposite is true, since the capacity is circa 155 mAh g^{-1} at the 30th cycle at C/20 rate in the same voltage range as in Fig. 7, against 180 mAh g^{-1} at C/10 rate according to Fig. 7. Nevertheless, the results in [68] were an improvement with respect to results prior to 2013, which the authors attributed to a modification in the lithium insertion mechanism that is no longer attributable to a two-phase reaction between the two-end

members $Li_{\varepsilon}TiO_2$ and $Li_{0.5\pm\alpha}TiO_2$ when downsizing the particle; instead, the insertion mechanism would proceed through a complete solid solution all along the composition range [69]. Indeed, in this prior work, the voltage plateau characteristic of the two-phase behavior in Fig. 6 was replaced by a continuous slope between the end members. However, the results obtained on 4-nm thick particles in Ref. [67] do show the same plateau as in Fig. 6. Therefore, the shift of the insertion mechanism from two-phase to a complete solid solution is not an intrinsic property linked to the size of the particles. A possible explanation is that the surface layer of the particles in Ref. [68] is ill-crystallized. In the case of $LiFePO_4$, for instance, we have determined that the amorphization of the surface layer also favors the solid-solution process, the two-phase behavior being recovered by heat treatment at circa 650 °C, accompanied with the re-crystallization of the surface layer during the carbon coating [70-72]. We believe the same disordered surface layer explains the results in Ref. [68]. In that case, however, the particle size that has been determined by the Scherrer formula has been underestimated, because the X-ray diffraction will probe only the crystallized part, i.e. the bulk part of radius 2 nm, to which the thickness of the more or less amorphous layer that is not probed by XRD should be added. If the thickness of the surface layer is about 2 nm, which is the typical size in $LiFePO_4$, the thickness of the particles might be circa 8 nm, intermediate between 4 nm in Ref. [67] and 20 nm in the present work. In any case, the decrease of the electrochemical performance in Ref. [68] with respect to the present case, let alone with respect to [61], clearly shows that the size of the particle is not the only pertinent parameter, and the quality of the surface is crucial. In addition, electrochemical properties even better than in Ref. [67] have also been obtained with larger particles of size 9 nm in [66]. We also note that good results obtained on N-doped carbon coated TiO_2 in [61] (even if the cyclability has been tested on only 60 cycles against 500 cycles in [67]) have been obtained with big spherical particles of size 550 nm. Therefore, even though the decrease of the size down to 4 nm may contribute to the outstanding performance in [67], the results obtained in the present work suggest that the main reason is a surface effect. In particular, the fragmentation of nanorods perpendicular to the direction allows to obtain a well-crystallized surface layer with an increased (001)/(101) facet ratio.

Due to the high energy surface of TiO_2, the nanoparticles show a tendency to self-aggregate during the charge-discharge process, and this is the main cause of the decay of the capacity upon cycling [73]. The best results have been obtained with special morphologies that avoid this irregular aggregation: one example is hollow nanostructures composed of nanosized primary building blocks [74]. The shell of the hollow structure was constructed by

nanoparticles with size of about 10–20 nm comparable to that of the particles in the present work. However, in virtue of the hollow structure and porosity of the shell, the self-aggregation was avoided. This electrode delivered a very stable discharge capacity of 150 mAh g^{-1} over 500 cycles that have been tested at 5C rate, despite the fact that it was rutile TiO_2, the phase that has the highest thermodynamic stability, but also considered as a poor Li^+-insertion material compared with the anatase phase. Another successful morphology is a hierarchical structure of micro/nanoparticles constructed by ultra-fine nanowires with 3–8 nm width and several micrometers length [75]. A capacity of 207 mAh g^{-1} was obtained at 0.2C after 150 cycles, and was maintained at 140 mAh g^{-1} at 25C. The authors have attributed this performance to the fact that, in such a kind of hierarchical structure, the micrometer dimensions of the architectural skeleton effectively avoid aggregation of the nanostructured active materials.

Conclusion

TiO_2 nanoparticles were prepared by a simple and cheap sol-gel method with subsequent annealing at moderate temperature of 400 °C for 1 h. X-ray diffraction and Raman spectroscopy show that the pure anatase phase was obtained without any rutile component. The nano morphology of the regular shaped particles, 20 nm in size, was observed by TEM and electron diffraction. The electrochemical measurements were carried out in the potential range 1-3 V vs. Li metal at C/10 rate and show a high reversible capacity of the anatase nanoparticles. An initial discharge capacity of 221 mAh g^{-1} was obtained that corresponds to insertion of 0.66 mol of Li per formula unit, while after 30 cycles, the charge and discharge capacity slightly decreased to 182 and 174 mAh g^{-1}, respectively, providing a decreasing irreversible capacity of 8 mAh g^{-1}. The results also suggest that a control of the crystallization of the surface layer and its protection by coating will be the strategy to optimize the performance of anatase TiO_2 particles. The diffusion coefficients derived from the cycliv voltammetry measurements are 8.5×10^{-13} and 5.8×10^{-13} cm^2 s^{-1} for oxidation (Li extraction) and reduction (Li insertion), respectively.

These results also suggest that a control of the crystallization of the surface layer and its porosity by appropriate coating of nanoparticles in a morphology that avoids the self-aggregation during cycling will be the strategy to optimize the performance of anatase TiO_2 particles by increasing the cycle life. The present work suggests that further works should be pursued along this direction, and are more promising than the opposite attempt that can be recently found in the literature, i.e. coating other active materials with TiO_2 films.

References

1. Han B, Kim KJ, Hwang BM, Kim, SB, Park KW (2013) Single-crystalline rutile TiO_2 nanowires for improved lithium ion intercalation properties. J Power Sources 222:225-229
2. Liu CL, Wang Y, Zhang C, Li XS, Dong WS (2014) In situ synthesis of α-MoO_3/graphene composites as anode materials for lithium ion battery. Mater Chem Phys 143:1111-1118
3. Julien CM, Mauger A, Vijh A, Zaghib K (2016) Lithium batteries:science and technology. Springer, Cham, Switzerland. 630 pages
4. Doh CH, Kim DH, Kim HS, Shin HM, Jeong YD, Moon SI, Jin BS, Eom SW, Kim HS, Kim KW, Oh DH, Veluchamy A (2008)Thermal and electrochemical behavior of C/Li_xCoO_2 cell during safety test. J Power Sources 175:881-885
5. Endo M, Kim C, Nishimura K, Fujino T, Miyashita K (2000) Recent development of carbon materials for Li ion batteries. Carbon 38:183–197
6. Qiao H, Xiao L, Zhang L (2008) Phosphatization: A promising approach to enhance the performance of mesoporous TiO_2 anode for lithium ion batteries. Electrochem Commun 10:616–620
7. Huang XH, Tu JP, Zhang CQ, Xiang JY (2007) Net-structured NiO–C nanocomposite as Li-intercalation electrode material. Electrochem Commun 9:1180–1184
8. Oh SW, Bang HJ, Bae YC, Sun YK (2007) Effect of calcination temperature on morphology, crystallinity and electrochemical properties of nano-crystalline metal oxides (Co_3O_4, CuO, and NiO) prepared via ultrasonic spray pyrolysis. J Power Sources 173:502–509
9. Chen G, Rodriguez R, Fei L, Xu Y, Deng S, Smirnov S, Luo H (2014) A facile hydrothermal route to iron(III) with conductive additives as composite anode for lithium ion batteries. J Power Sources 259:227-232
10. Xu Y, Jian G, Liu Y, Zhu Y, Zachariah MR, Wang C (2014) Superior electrochemical performance and structure evolution of mesoporous Fe_2O_3 anodes for lithium-ion batteries. Nano Energy 3:26–35
11. Oh HD, Lee SW, Kim SO, Lee JK (2013) Facile synthesis of carbon layer-entangled Fe_2O_3 clusters as anode materials for improved Li-ion batteries. J Power Sources 244:575-580

12. Jiang Y, Zhang D, Li Y, Yuan T, Bahlawane N, Liang C, Sun W, Lu Y, Yan M (2014) AmorphousFe_2O_3 as a high-capacity, high-rate and long-life anode material for lithium ion batteries. Nano Energy 4:23–30
13. Casino S, Di Lupo F, Francia C, Tuel A, Bodoardo S, Gerbaldi C (2014) Surfactant-assisted sol gel preparation of high-surface area mesoporous TiO_2 nanocrystalline Li-ion battery anodes. J Alloys Compd 594:114–121
14. Di Lupo F, Tuel A, Mendez V, Francia C, Meligrana G, Bodoardo S, Gerbaldi C (2014) Mesoporous TiO_2 nanocrystals produced by a fast hydrolytic process as high-rate long-lasting Li-ion battery anodes. Acta Mater 69:60–67
15. Wang D, Wu X, Zhang Y, Wang J, Yan P, Zhang C, He D (2014) The influence ofTiO_2 particle size on the properties of $Li_4Ti_5O_{12}$ anode material for lithium-ion battery. Ceramics Int 40:3799–3804
16. Usui H, Wasada K, Shimizu M, Sakaguchi H (2013) TiO_2/Si composites synthesized by sol–gel method and their improved electrode performance as Li-ion battery anodes. Electrochim Acta 111:575– 580
17. Yan Y, Wang J, Chang Q, Babikier M, Wang H, Li H, Yu Q, Gao S, Jiao S (2013) Fabrication of mesoporous TiO_2 electrodes by chemical technique for dye-sensitized solar cells. Electrochim Acta 94:277–284
18. Chen CL, Chang TW, Su SC, Teng H, Lee YL (2014) High performance solid-state dye-sensitized solar cells based on poly(acrylonitrile-co-vinyl acetate)/TiO_2 nanoparticles redox electrolytes. J Power Sources 247:406-411
19. Hong CK, Jung YH, Kim HJ, Park KH (2014) Electrochemical properties of TiO_2 nanoparticle/nanorod composite photoanode for dye-sensitized solar cells. Current Appl Phys 14:294-299
20. Xiong J, Yang B, Zhou C, Yang J, Duan H, Huang W, Zhang X, Xia X, Zhang L, Huang H, Gao Y (2014) Enhanced efficiency and stability of polymer solar cells with TiO_2 nanoparticles buffer layer. Organ Electron 15:835–843
21. Umar AA, Nafisah S, Saad SKM, Tan ST, Balouch A, Salleh M, Oyama M (2014) Pori ferous microtablet of anatase TiO_2 growth on an ITO surface for high efficiency dye-sensitized solar cells. Solar Energy Mater Solar Cells 122:174–182
22. Zhang S, Zhang S, Peng B, Wang H, Yu H, Wang H, Peng F (2014) High performance hydrogenated TiO_2 nanorod arrays as a photoelectrochemical sensor for organic compounds under visible light. Electrochem Commun 40:24–27

23. Lee HU, Lee SC, Lee SM, Lee JW, Kim HJ, Lee J (2013) Improved photocatalytic and antibacterial activities of three-dimensional polycrystalline anatase TiO_2 photocatalysts. Appl Catalysis A 467:394–399
24. Lee AC, Lin RH, Yang CY, Lin MH, Wang WY (2008) Preparations and characterization of novel photocatalysts with mesoporous titanium dioxide (TiO_2) via a sol–gel method. Mater Chem Phys 109:275–280
25. Xie Y, Wu Z, Wu Q, Liu M, Piao L (2014) Effect of different base structures on the performance of the hierarchical TiO_2 photocatalysts. Catalysis Today 225:74– 79
26. Lee HU, Lee SC, Cho SH, Son B, Lee SJ, Kim HJ, Lee J (2013) Highly visible-light active nanoporous TiO_2 photocatalysts for efficient solar photocatalytic applications. Applied Catalysis B: Environmental 129:106– 113
27. Zhang L, Xu L, Wang J, Cai J, Xu J, Zhou H, Zhong Y, Chen D, Zhang J, Cao CN (2012) Enhanced energy storage of a UV-irradiated three-dimensional nanostructured TiO_2–$Ni(OH)_2$ composite film and its electrochemical discharge in the dark. J Electroanal Chem 683:55–61
28. Rai AK, Anh LT, Gim J, Mathew V, Kang J, Paul BJ, Song J, Kim J (2013) Simple synthesis and particle size effects of TiO_2 nanoparticle anodes for rechargeable lithium ion batteries. Electrochim Acta 90:112-118
29. Yang X, Teng D, Liu B, Yu Y, Yang X (2011) Nanosized anatase titanium dioxide loaded porous carbon nanofiber webs as anode materials for lithium-ion batteries. Electrochem Commun 13:1098-1101
30. Qiao H, Xiao L, Zhang L (2008) Phosphatization: a promising approach to enhance the performance of mesoporous TiO_2 anode for lithium ion batteries. Electrochem Commun 10:616-620
31. Oh SW, Park SH, Sun YK (2006) Hydrothermal synthesis of nano-sized anatase TiO_2 powders for lithium secondary anode materials. J Power Sources 161:1314–1318
32. Subramanian V, Karki A, Gnanasekar KI, Eddy FP, Rambabu B (2006) Nanocrystalline TiO_2 (anatase) for Li-ion batteries. J Power Sources 159:186–192
33. Liu G, Qu J, Wang H (2013) Morphology-control synthesis and electrochemical performance of titanate and anatase TiO_2. J Alloys Compd 578:345–348
34. Choi MG, Lee YG, Song SW, Kim KM (2010) Lithium-ion battery anode properties of TiO_2 nanotubes prepared by the hydrothermal synthesis of mixed (anatase and rutile) particles. Electrochim Acta 55:5975–5983

35. Casino S, Di Lupo F, Francia C, Tuel A, Bodoardo S, Gerbaldi C (2014) Surfactant-assisted sol gel preparation of high-surface area mesoporous TiO_2 nanocrystalline Li-ion battery anodes. J Alloys Compd 594:114–121
36. Lin KS, Cheng HW, Chen WR, Wu JF (2010) Synthesis, characterization and application of anatase-typed titania nanoparticles. J Environ Eng Manag 20:69-76
37. Deedar N, Irfan A, Ishtiaq Q (2009) Evaluation of the adsorption potential of titanium dioxide nanoparticles for arsenic removal. J Environm Sci 21:402-408
38. Li Z, Hong L, Guo B (2005) Physicochemical and electrochemical characterization of anatase titanium dioxide nanoparticles. J Power Sources 143:231-235
39. Kun G (2007) Strongly intrinsic anharmonicity in the low-frequency Raman mode in nanocrystalline anatase TiO_2. Physica B 398:33–37
40. Orendorz A, Brodyanski A, Losch J, Bai LH, Chen ZH, Le YK, Ziegler C, Gnaser H (2007) Phase transformation and particle growth in nanocrystalline anatase TiO_2 films analyzed by X-ray diffraction and Raman spectroscopy. Surf Sci 601:4390–4394
41. Cheng G, Akhtar MS, Yang O-B, Stadler FJ (2013) Structure modification of anatase TiO_2 nanomaterials-based photoanodes for efficient dye-sensitized solar cells. Electrochim Acta 113:527–535
42. Exnar I, Kavan L, Huang SY, Gratzel M (1997) Novel 2 V rocking-chair lithium battery based on nano-crystalline titanium dioxide. J Power Sources 68:720-722
43. Kavan L, Tathousky J, Gratzel M, Shklover V, Zukal A (2000) Surfactant-templated TiO_2 (anatase), characteristic features of lithium insertion electrochemistry in organized nanostructures. J Phys Chem B 104:12012-12020
44. Cava RJ, Murphy DW, Zahurak S, Santoro A, Roth RS (1984) The crystal structures of the lithium-inserted metal oxides $Li_{0.5}TiO_2$ anatase, $LiTi_2O_4$. J Solid State Chem 53:64-75
45. Yang Z, Choi D, Kerisit S, Rosso KM, Wang D, Zhang J, Graff G; Liu, J (2009) Nanostructures and lithium electrochemical reactivity of lithium titanites and tinanium oxides. J Power Sources 192:588−598
46. Kim J, Cho J (2007) Rate characteristics of anatase TiO_2 nanotubes and nanorods for lithium battery anode materials at room temperature. J Electrochem Soc 154:A542–A546
47. Luttrell T, Halpegamage S, Tao J, Kramer A, Sutter E, Batzill M (2014) Why is anatase a better photocatalyst than rutile? Model studies on epitaxial TiO_2 films. Sci Rep 4:4043
48. Brinker CJ, Hurd AJ, Schunk PR, Frye GC, Ashley CS (1992) Review of sol-gel thin film formation. J Non-Crystal Solids 147-148:424-436

49. Tan L, Cao C, Yang H, Wang B, Li L (2013) Nitrogen-doped carbon coated TiO_2 anode material for lithium-ion batteries. Mater Lett 109:195-198
50. Levi MD, Salitra G, Markovsky B, Teller H, Aurbach D, Heider U, Heider L (1999) Solid-state electrochemical kinetics of Li-ion intercalation into $Li_{1-x}CoO_2$: Simultaneous application of electroanalytical techniques SSCV, PITT, and EIS. J Electrochem Soc 146:1279-1289
51. Kanamura K, Yuasa K, Takehara Z (1987) Diffusion of lithium in the TiO_2 cathode of a lithium battery. J Power Sources 20:127-134
52. Cantao MP, Cisneros JI, Torresi RM (1994) Kinetic study of lithium electroinsertion in titanium oxide thin films. J Phys Chem 98:4865-4869
53. Lindstrom H, Sodergren S, Solbrand A, Rensmo H, Hjelm J, Hagfeldt A, Lindquist S (1997) Li^+ ion insertion in TiO_2 (anatase). 2. Voltammetry on nanoporous films. J Phys Chem B 101:7717–7722
54. Lindstrom H, Sodergren S, Solbrand A, Rensmo H, Hjelm J, Hagfeldt A, Lindquist, S (1997) Li^+ ion insertion in TiO_2 (anatase). 1. Chronoamperometry on CVD films and nanoporous films. J Phys Chem B 101:7710–7716
55. Kavan L, Grätzel M, Gilbert SE, Klemenz C, Scheel HJ (1996) Electrochemical and photoelectrochemical investigation of single-crystal anatase. J Am Chem Soc 118:6716-6723
56. Wagemaker M, Van de Krol R, Kentgens APM, van Well AA, Mulder FM (2001) Two phase morphology limits lithium diffusion in TiO_2 (anatase): a ^7Li MAS NMR study. J Am Chem Soc 123:11454-11461
57. Dylla AG, Lee JA, Stevenson KJ (2012) Influence of mesoporosity on lithium-ion storage capacity and rate performance of nanostructured TiO_2(B). Langmuir 28 (2012) 2897-2903
58. Zec N, Cvjeticanin N, Bester-Rogac M, Vranes M, Gadzuric S (2017) Electrochemical performance of anatase TiO_2 nanotube arrays electrode in ionic liquid based electrolyte for lithium ion batteries. J Electrochem Soc 164:H5100-H5107
59. Tan L, Pan L, Cao C, Wang B, Li L (2014) Nitrogen-doped carbon coated TiO_2 nanocomposites as anode material to improve cycle life for lithium-ion batteries. J Power Sources 253:193-200
60. Liu Y, Yang Y (2016) Recent progress of TiO_2-based anodes for Li ion batteries, J. Nanomaterials 2016:8123652

61. Y. Fu, H. Ming, Q. Zhou, L. Jin, X. Li, J. Zheng (2014) Nitrogen-doped carbon coating inside porous TiO_2 using small nitrogen-containing molecules for improving performance of lithium-ion batteries Electrochim Acta 134:478-485

62. S. Li, P. Ge, C. Zhang, W. Sun, H. Hou, X. Ji (2017). The electrochemical exploration of double carbon-wrapped $Na_3V_2(PO_4)_3$: Towards long-time cycling and superior rate sodium-ion battery cathode. J Power Sources 366:249-258

63. Rod like Sb_2Se_3 Wrapped with Carbon: The Exploring of Electrochemical Properties in Sodium-Ion Batteries. P. Ge, X. Cao, H. Hou, S. Li, X. Ji, ACS Appl Mater Interfaces 9: 34979-34989

64. P. Ge, H. Hou, X. Ji, Z. Huang, S. Li, L. Huang (2018) Enhanced stability of sodium storage exhibited by carbon coated Sb_2S_3 hollow spheres. Mater Chem Phys 203:185-192.

65. W. Zhou, F. Sun, K. Pan, G. Tian, B. Jiang, Z. Ren, C. Tian, H. Fu (2011) Well-ordered large-pore mesoporous anatase TiO_2 with remarkably high thermal stability and improved crystallinity: preparation, characterization, and photocatalytic performance. Adv Func Mater 21 (2011) 1922

66. X. Bai, T. Li, Y.-X. Qi, Y.-X. Wang, L.-W. Yin, H. Li, N. Lun, Y.-J. Bai (2016) One-step fabricating nitrogen-doped TiO_2 nanoparticles coated with carbon to achieve excellent high-rate lithium storage performance. Electrochim Acta 187:389-396

67. Bresser D, Kim G-T, Binetti E, Striccoli M, Comparelli R, Seidel S, Ozkaya D, Copley M, Bishop P, Paillard E, Passerini S (2015) Transforming anatase TiO_2 nanorods into ultrafine nanoparticles for advanced electrochemical performance. J Power Sources 294:406-413

68. Patra S, Davoisne C, Bouyanfif H, Foix D, Sauvage F (2015) Phase stability frustration on ultra-nanosized anatase TiO_2. Sci Rep 5:10928

69. Patra S, Davoisne C, Bruyre S, Bouyanfif H, Cassaignon S, Taberna P-L, Sauvage F (2013) Room-temperature synthesis of high surface area anatase TiO_2 exhibiting a complete lithium insertion solid solution. Part Part Syst Char 30:1093-1104

70. Zaghib K, Mauger A, Gendron F, Julien CM (2008) Surface effects on the physical and electrochemical properties of thin $LiFePO_4$ particles. Chem Mat 20:462-469

71. Zaghib K, Charest P, Dontigny M, Guerfi A, Lagac. M, Mauger A, Kopec M, Julien CM (2010) $LiFePO_4$: from molten ingot to nanoparticles with high-rate performance in Li-ion batteries. J Power Sources 195:8280–8288

72. Trudeau ML, Laul D, Veillette R, Serventi AM, Mauger A, Julien CM, Zaghib K (2011) In situ high-resolution transmission electron microscopy synthesis observation of nanostructured carbon coated $LiFePO_4$. J Power Sources 196:7386-7394.

73. Guo BJ, Yu K, Fu H, Hua QQ, Qi RJ, Li HL, Song HL, Guo S, Zhu ZQ (2015) Firework-shaped TiO_2 microspheres embedded with few-layer MoS_2 as an anode material for excellent performance lithium-ion batteries. J Mater Chem A 3:6392-6401

74. Yu XY, Wu HB, Yu L, Ma FX, Lou XW (2015) Rutile TiO_2 submicroboxes with superior lithium storage properties. Angew Chem 54:4001-4004

75. Tian Q, Zhang Z, Yang L, Hirano SI (2015) Morphology-engineered and TiO_2(B)-introduced anatase TiO_2 as an advanced anode material for lithium-ion batteries, J Mater Chem A 3:14721-14730